NASA

Technical Memorandum 83877

Sensitivity of a Climatologically - Driven Sea Ice Model to the Ocean Heat Flux

Claire L. Parkinson and Michael R. Good

JANUARY 1982

National Aeronautics and Space Administration

Goddard Space Flight Center
Greenbelt, Maryland 20771

SENSITIVITY OF A CLIMATOLOGICALLY-DRIVEN SEA ICE MODEL TO THE OCEAN HEAT FLUX

Claire L. Parkinson
Goddard Laboratory for Atmospheric Sciences
NASA/Goddard Space Flight Center
Greenbelt, MD 20771

Michael R. Good
Computer Sciences Corporation
8728 Colesville Road
Silver Spring, MD 20910
and
Goddard Laboratory for Atmospheric Sciences
NASA/Goddard Space Flight Center
Greenbelt, MD 20771

January 1982

GODDARD SPACE FLIGHT CENTER

Greenbelt, Maryland 20771

SENSITIVITY OF A CLIMATOLOGICALLY-DRIVEN SEA ICE MODEL TO THE OCEAN HEAT FLUX

Claire L. Parkinson
Goddard Laboratory for Atmospheric Sciences
NASA/Goddard Space Flight Center
Greenbelt, MD 20771

Michael R. Good
Computer Sciences Corporation
8728 Colesville Road
Silver Spring, MD 20910
and
Goddard Laboratory for Atmospheric Sciences
NASA/Goddard Space Flight Center
Greenbelt, MD 20771

Abstract

A set of ocean-heat-flux sensitivity studies has been performed on a numerical model of sea ice covering the Weddell Sea region of the southern ocean. The model is driven by mean-monthly climatological atmospheric variables; it contains an 8-hour timestep and a 200-kilometer horizontal resolution; and the simulations proceed from January of year 1 through February of year 2. For each model run, the ocean heat flux is uniform in both space and time. In a series of six model runs, this flux magnitude has been varied from 0 to 40 W m^{-2}, with the result that, in these climatologically-driven simulations, a value of 25 W m^{-2} yields the most realistic sea ice distributions. Ocean heat fluxes below 20 W m^{-2} do not provide sufficient energy to allow the ice to melt to its summertime thicknesses and concentrations by the end of the 14-month simulation, whereas ocean heat fluxes of 30 W m^{-2} and above result in too much ice melt, producing the almost total disappearance of ice in the Weddell Sea by the end of the 14 months. These results, however, are strongly dependent on the atmospheric forcing fields.

CONTENTS

SENSITIVITY OF A CLIMATOLOGICALLY-DRIVEN SEA ICE MODEL TO THE OCEAN HEAT FLUX

I. INTRODUCTION

In an ice-covered region of the ocean, the flux of heat from the water beneath to the bottom of the ice can be significant in determining the amount of bottom melt and in affecting the seasonal cycle, thickness, and distribution of the sea ice cover. Calculations by Gordon (1981) indicate that, in the 60°S - 70°S latitude band of the southern ocean, roughly half the heat required for the observed November to January decay of the ice cover must derive from the relatively warm water below the pycnocline.

When Parkinson and Washington (1979) modeled the global sea ice cover, they employed values of 2 W m^{-2} for the ocean heat flux in the northern hemisphere and 25 W m^{-2} for the flux in the southern hemisphere. The 2 W m^{-2} northern hemisphere value was taken directly from modeling studies of Maykut and Untersteiner (1971) and was initially used for both hemispheres. This value, however, proved satisfactory for the Arctic simulation but very unsatisfactory for the Antarctic simulation. It was clear that a much larger heat flux was required to keep the simulated Antarctic ice within the bounds of the observed ice cover. This modeling indication of a larger vertical ocean heat flux in the southern ocean than the 2 W m^{-2} used for the Arctic is in line with recent southern ocean estimates (e.g., the 31 W m^{-2} estimated by Gordon (1981) for the deep water to surface water flux).

It is probably not legitimate, though, to interpret the model results as determining the magnitude of the actual ocean flux. This is especially true in view of the smoothed, mean monthly climatological values employed

for the atmospheric variables. Hence, in this paper the emphasis lies not in determining the actual ocean heat flux but rather in the more modest task of examining the sensitivity of the calculated sea ice distributions to the specific value used for that flux. Toward this end, use is made of a modified version of the Parkinson and Washington model in obtaining a sequence of six 14-month simulations. Over the six model runs, all conditions remain identical except the ocean heat flux, which assumes values of 0, 10, 20, 25, 30, and 40 W m^{-2} for the six cases.

II. MODEL AND PROCEDURE

The numerical model used for the present study is a modification of the Parkinson and Washington (1979) model of the seasonal cycle of sea ice in the northern and southern hemispheres. In both the original and the modified version, the model accounts for thermodynamic changes in the ice through energy balances at the water-ice, ice-snow, and snow-air interfaces and accounts for ice dynamics through a momentum equation and an adjustment for internal ice resistance. The momentum equation incorporates air stress, water stress, dynamic topography, and Coriolis force, whereas the energy balances incorporate incident and reflected solar radiation, incoming and outgoing longwave radiation, sensible and latent heat fluxes, conduction through the ice and snow layers, and the flux of energy--termed the ocean heat flux--from the water to the undersurface of the ice. Areal percentages of leads within each grid square are also calculated through energy balance considerations. Details of the calculations can be found in Parkinson and Washington (1979), hereafter referred to as P & W.

Included among the aspects retained from the P & W model are the 8-hour timestep, the 30-day months, the approximately 200 km horizontal

resolution, the insistence on at least a 2% lead fraction in each grid square, and the use, for the atmospheric variables, of mean monthly climatological fields linearly interpolated for the individual timesteps. The following changes, however, have been made from the P & W version:

(1) The model grid has been reduced to a 23 x 17 subset of the full 41 x 41 P & W grid, thus allowing inexpensive testing of the sensitivity of the model. The 23 x 17 subset covers the Weddell Sea region of the southern ocean (Figure 1).

(2) The model runs are for 14-month simulations, in contrast to the 4-year simulations of P & W.

(3) The initial conditions have been extensively revised, becoming more realistic. In the P & W work the model was everywhere initialized with 90% coverage of 1.5 m thick ice, an excessive ice amount which was allowed to decrease through 4 simulation years, thereby reaching an approximate equilibrium. In the current work, the shorter simulation period (above) necessitates setting the initial conditions more realistically. Consequently, ice concentrations are initialized at values derived from brightness temperatures recorded by the Electrically Scanning Microwave Radiometer (ESMR) on the Nimbus 5 satellite. This instrument and data from it have been described by Wilheit (1972) and by Zwally et al. (1976). Ice thicknesses plus the temperatures of the upper snow surface and of the snow-ice interface for each grid square are all initialized from the simulated values at the completion of a 4-year run of the P & W model, with appropriate modifications for consistency with the satellite ice concentrations. [If the concentration is 0%, then the ice thickness is set at 0 m, the snow surface temperature is set at 273.15 K, and the snow-ice interface temperature is set at 273.05 K. If the

ice concentration is positive, then the temperature of the water is set at 271.2 K.] Finally, ocean temperatures are initialized from summertime 20 m ocean temperatures of Gordon and Goldberg (1970). Each of these five input fields is mapped in Figure 2. As in the P & W work, the snow cover is initialized everywhere at 0.0 m, and the temperature of the water under the ice is initialized everywhere at 271.2 K.

(4) The snowfall rate has been increased from 1.1574×10^{-9} m s^{-1} for the 9 months from March through November to 8.57×10^{-9} m s^{-1} for the same 9 months. This increases the yearly snowfall from 2.7 cm to 20 cm. Also, the snow covering the ice is now advected along with the ice.

(5) The value of ice thickness upon initial freezing in a grid square of 0% ice concentration has been increased from 1 cm to 10 cm. As before, the ice concentration is then calculated from the energy deficit in the grid square and the assumed initial thickness by insisting that the volume of water frozen is that volume which releases the amount of heat to match the calculated heat deficit.

(6) The ocean heat flux to the undersurface of the ice is now applied to the lead area as well. Essentially, this flux is perceived as deriving from the deeper ocean. The model's sensitivity to the magnitude of the ocean flux constitutes the central topic of this paper.

The model has been run for six 14-month simulations, the six cases assuming ocean heat flux values of 0, 10, 20, 25, 30, and 40 W m^{-2}, respectively. Contour maps of simulated ice thicknesses and ice concentrations were drawn for the middle of each month and the following variables were plotted as a function of time: (1) ice thicknesses and concentrations at 2 individual points, located at (9,4) and (5,7) on the grid; (2) ice thicknesses and concentrations averaged over those grid squares containing

some ice (labelled 'ice-laden'); (3) the area of ice-laden waters; and (4) the 'cumulative' ice area, this being the area of actual ice coverage.

III. RESULTS

a. Spatial Plots

Figures 3-8 present contours of ice thickness and ice concentration for months 2, 8, and 14, i.e., for February (months 2 and 14), the month of minimum Antarctic ice, and for August, a peak winter month. The maps show a fairly smooth transition from the case with no ocean heat flux to the case with a flux of 40 W m^{-2}, the greater flux naturally resulting in more melt and hence lesser ice thickness and lesser ice extent. Since mean climatological data are employed, if all the inputs, including the ocean heat flux, were realistic, the February thickness and concentration fields would not vary greatly from the first year to the second. Clearly this is not the case when the ocean heat flux is 0 or 10 W m^{-2}, these flux amounts being insufficient for melting the requisite ice amount (Figures 3-4 and 7-8). With zero ocean flux, the maximum thicknesses are even greater in the second February than at the peak of winter (August, Figure 5). Even in this case, though, the ice extents remain less in February than in August, showing that the model does simulate summertime ice edge retreat even with the ocean heat flux eliminated and with ice thickening continuing in some of the inner regions of the pack (see, for instance, Figure 11).

When the heat flux is increased to 40 W m^{-2}, the ice entirely disappears by January and February of the second year (Figures 7 and 8; for January, see Figure 16). In the 30 W m^{-2} case, some ice remains in the second February, but the amount is unrealistically small and is much less than would be necessary for an equilibrium between the first and second

Februaries (Figures 3-4 versus 7-8). This leaves the two cases employing ocean heat fluxes of 20 and 25 W m^{-2}. The 25 W m^{-2} case comes closer to reestablishing in month 14 the ice conditions existent in month 2, i.e., to reaching an equilibrium yearly cycle. This case is our "standard" and will be used for comparison purposes in Figures 9-16. The 25 W m^{-2} value is also the value used by P & W for the ocean heat flux.

In August (Figures 5 and 6), even with a heat flux as great as 40 W m^{-2}, the simulated ice covers the majority of the grid. Less than half of this ice, however, has a thickness exceeding 20 cm. One interesting feature of these mid-winter results is the substantial area of reduced ice concentrations midway through the pack to the east of the prime meridian. These anomalously low ice concentrations, found in each of the six cases, occur in the approximate location of the 1974 Weddell Polynya observed from Nimbus 5 ESMR data (Carsey, 1980). This is a favorable correspondence of the model with the observations, even though it is only with ocean fluxes of at least 30 W m^{-2} that the model obtains concentrations low enough to indicate a true polynya.

Except in the region of reduced ice concentrations near the 1974 Weddell Polynya site, the ocean heat flux variations inserted into the model generally have a greater influence on ice thicknesses than on ice concentrations. This was expected, since in the model the ocean flux directly melts the ice vertically but only indirectly melts it laterally through the warming of the ocean mixed layer.

Maximum August thicknesses decrease from 2.3 m for zero ocean heat flux to 0.7 m for an ocean flux of 40 W m^{-2}. In all six cases the thickness gradient is basically positive from north to south, with some tendency for the slopes to steepen poleward. Concentrations, by contrast,

remain predominantly above 90% even with the largest ocean heat fluxes, and the steepest slopes occur at the equatorward edge. Because high heat flux values can reduce ice concentrations to 0% abruptly by decreasing ice thicknesses to 0 m, the sharpness of the 0% - 90% concentration gradient tends to be greater for the higher heat flux values. Still, the latitudinal position of the outer ice edge varies for most regions by less than 4° over the six case studies, with the largest contrasts in extent occurring in the vicinity of the Antarctic Peninsula.

b. Time Sequences

Two grid points have been selected for more specific examination of the thickness and concentration trends through the 14 months. These points, at positions (5,7) and (9,4), are northeast of the Peninsula (at 62°S, 312°W) and deep within the Weddell Sea (at 71°S. 315°W), respectively. This places one point in a region which is often free of ice in summer and the other point in a region remaining ice-covered in all seasons. Both points are indicated on Figure 1.

At (5,7), ice forms in May in each of the six cases but disappears in early October with an ocean flux of 40 W m^{-2}, in November with ocean fluxes of 25 or 30 W m^{-2}, in December with a flux of 20 W m^{-2}, and not at all with fluxes of 0 - 10 W m^{-2} (Figures 9 and 10). This contrast from less than 1 months' difference in the timing of ice formation to greater than 5 months' difference in the timing of ice disappearance derives from both (a) the lesser influence of the ocean heat flux on the modelled ocean temperature compared to the greater influence on the melting at the undersurface of the ice, and (b) the cumulative effect as the simulation proceeds. Because of the strong influence of the ocean flux on bottom melt, a substantial variation exists in the maximum thickness reached at this

location in the six cases, varying from just over 1.1 m when no ocean flux is allowed to about 0.2 m when the flux is 40 W m^{-2}. The generally smooth growth-decay cycle in the thickness curves is disrupted in the two lowest flux cases by an anomalous thickening of the ice beginning in early January of the second year. This results not from an anomaly in the air temperatures or solar radiation but from ice advection into point (5,7) from an adjacent grid point with thicker ice. By contrast, the abrupt decreases of ice thickness to 0 m in early December and late November of the 20 and 25 W m^{-2} cases, respectively, are not due to advection out of the grid square but to lateral ice melt. This lateral ice melt is clear from the concentration decreases of Figure 10.

At (9,4), ice remains throughout the year for all cases with an ocean flux no greater than 25 W m^{-2}, but it disappears in mid January of the second simulation year when the ocean flux is 30 W m^{-2} and in early December of the first year when the flux is 40 W m^{-2} (Figures 11 and 12). The zero flux case has--unrealistically--no summer thinning. In terms of reaching an equilibrium, with January and February of the second year approximating January and February of the first year, of the six cases presented, the 25 W m^{-2} ocean flux case comes closest to an equilibrium for thicknesses at point (9,4), with the indications being that a slightly higher heat flux is desired (Figure 11a). The same 25 W m^{-2} case also comes closest to an equilibrium for ice concentrations at (9,4), though for concentrations the indications are that a somewhat lower flux might be preferable, especially for the January equilibrium (Figure 12a). The summer disappearance of ice for the 30 and 40 W m^{-2} cases is unrealistic for this location.

For a less geographically-limited indication of the influence of

the ocean heat flux, several variables have been examined in terms of a total or average value over the entire ocean portion of the grid from 300°E to 20°E (Figure 1). This region is the Weddell Sector in the Zwally et al. (1979) sectorization of the southern ocean. The variables examined for this sector are the total area of ice-laden waters, the average ice thickness, the average ice concentration, and the total area of actual ice coverage (deleting, for this last variable, the open water areas within the pack).

In the simulation results, there is a realistic peaking of the area of ice-laden waters in August or September for each of the six cases, with earlier (and lower) peaks occurring for the higher ocean heat fluxes (Figure 13). It is interesting that, although the greater ocean heat fluxes result in a significantly lower minimum area of ice (the late February and early March values in the case of 40 W m^{-2} ocean flux being less than half those of the 0 W m^{-2} case), the March and April growth rate is actually faster with the higher fluxes, so that the late April values are closer for the six cases than are the values in the preceding two and a half months. From late April until the end of the simulation the curves for the six cases diverge, a process especially noticeable after the time of maximum area of ice-laden waters. Once again, the 25 W m^{-2} case comes closest to stabilizing over the 14-month simulation. Since the February, year 2 ice-laden-water area is slightly higher than the February, year 1 value for the 25 W m^{-2} case, a slightly higher flux (26-27 W m^{-2}) might further improve the stabilization.

Time sequences of average ice thickness over the Weddell Sector (Figure 14) show comparable but slightly different results from the sequences of ice-laden-water area. Regarding stabilization, the average thickness curves

suggest that an ocean heat flux between 20 and 25 W m^{-2} would be necessary for attaining equilibrium (Figure 14). The 20 W m^{-2} curve most closely reproduces the February, year 1 values in February of year 2; however, the 25 W m^{-2} curve most closely reproduces the model's initial value by the start of the second year.

In contrast to the area of ice-laden waters (Figure 13), the average thicknesses do not retain the seasonal contrast of low summer values and high winter values. This is largely because the thicknesses are being averaged only over the changing ice-covered portion of the Weddell Sector rather than over the sector as a whole. This complicates the interpretation somewhat. For instance, the decrease in the average thickness from April through June, apparent in each of the six cases (Figure 14), does not result from a thinning of the ice over these ice-growth months but from the strong increase in the area of ice-laden waters (Figure 13). As the area increases, very thin emerging ice artificially depresses the overall average ice thickness. Interpretation of the curves for the average concentration in ice-laden grid squares (Figure 15) is similarly less straightforward than the interpretation of the curves for individual points (e.g., Figures 9-12). In fact, the average concentration curves do not even show the 0 W m^{-2} case to consistently have the highest concentrations and the 40 W m^{-2} case to consistently have the lowest concentrations, the reason being that the lesser number of ice-laden grid squares in the higher heat flux cases (reflected in Figure 13) permits the average concentrations in Figure 15 to exceed, in some months, the average concentrations for the cases with lesser ocean flux. Nonetheless, these curves do still provide substantial information on the average concentrations produced by the model and on the strong seasonal contrast in these average

concentrations. Average summertime concentrations (for the ice-laden 200 x 200 km grid squares) are about 10%, and average wintertime concentrations are about 90%. The effect of the ocean heat flux is almost negligible in the fall and early winter but becomes pronounced in the spring and summer melt season.

In contrast to the above cases of average ice thickness and average ice concentration, there is no corresponding ambiguity in the interpretation of the curves of cumulative ice area (Figure 16). Greater ocean heat flux leads to lesser cumulative area throughout the year. The two cases with January and February of the second year best matching January and February of the first year are those using fluxes of 20 and 25 W m^{-2}. In these cases the summertime cumulative ice area is about 0.2 x 10^6 km^2, which seems somewhat low, while the peak wintertime cumulative area is about 5.5 x 10^6 km^2, which seems quite realistic. ESMR satellite data for 1974 indicate a minimum cumulative ice area of about 0.8 x 10^6 km^2 and a maximum cumulative ice area of about 5.6 x 10^6 km^2.

IV. CONCLUSIONS

Large-scale uncertainty exists regarding the proper value of the vertical ocean heat flux in the southern ocean. Because this flux contributes to bottom ablation of the sea ice cover, it is important when modeling sea ice to use reasonable values for its magnitude. One method of estimating reasonable values is to insert several alternatives into the models in question and to examine the simulated ice concentrations and thicknesses. This has been done for six model runs of a climatologically-driven sea ice model with ocean heat fluxes ranging from 0 to 40 W m^{-2}.

Physical considerations indicate that the actual ocean heat flux varies both spatially and temporally. However, in view of the wide uncertainties

in the actual values, it was decided that the most direct method of examining the sensitivity of the sea ice model to the ocean flux would be accomplished by maintaining, for each model run, a flux which remains constant in both space and time. The simulation results indicate that within the 0 - 40 W m^{-2} range used for the ocean flux, the effect on the ice cover is significant. Ocean heat fluxes of 30 W m^{-2} and above result in almost the total disappearance of ice in the Weddell Sea by late summer, whereas fluxes below 20 W m^{-2} do not provide sufficient energy to melt the ice to reasonable summertime concentrations and extents. Results suggest a value of 25 W m^{-2} as a reasonable overall spatial-temporal average to use for the ocean heat flux in the given, climatologically-driven model. This does not imply, however, that 25 W m^{-2} is a reasonable value for the actual ocean flux. Although the model employs mean monthly climatological atmospheric variables, it is initialized with ice conditions specifically for the start of 1974, and the qualitative determination of which model simulations appear most reasonable depended largely on how the results compare with observed sea ice conditions in the mid-1970's. Preliminary attempts to use 1974 data with the same sea ice model as described above yield results which are comparable in terms of the sensitivity of the model but very different in terms of the specific ocean heat flux producing the most realistic simulations. The air temperature data used for 1974 is generally higher than the climatological temperature data, and hence a lower ocean heat flux is required to attain a comparable ice thickness.

ACKNOWLEDGEMENTS. This research was supported by the Climate and Oceanography Programs at NASA Headquarters.

REFERENCES

Carsey, F. D., 1980: Microwave observation of the Weddell Polynya. Monthly Weather Review, 108, 2032-2044.

Gordon, A. L., 1981: Seasonality of Southern Ocean sea ice. Journal of Geophysical Research, 86, 4193-4197.

Gordon, A. L. and R. D. Goldberg, 1970: Circumpolar characteristics of Antarctic waters. In: Antarctic Map Folio Series, Folio 13, ed. by V. V. Bushnell, American Geographical Society, New York.

Maykut, G. A. and N. Untersteiner, 1971: Some results from a time-dependent thermodynamic model of sea ice. Journal of Geophysical Research, 86, 4193-4197.

Parkinson, C. L. and W. M. Washington, 1979: A large-scale numerical model of sea ice. Journal of Geophysical Research, 84, 311-337.

Wilheit, T. T., 1972. The electrically scanning microwave radiometer (ESMR) experiment. Nimbus 5 User's Guide, NASA/Goddard Space Flight Center, Greenbelt, Maryland, 59-105.

Zwally, H. J., C. L. Parkinson, F. D. Carsey, P. Gloersen, W. J. Campbell, R. O. Ramseier, 1979: Antarctic sea ice variations 1973-75. In: Fourth National Aeronautics and Space Administration Weather and Climate Program Science Review, Goddard Space Flight Center, Greenbelt, Maryland. pp. 335-340.

Zwally, H. J., T. T. Wilheit, P. Gloersen, J. L. Mueller, 1976. Characteristics of Antarctic sea ice as determined by satellite-borne microwave imagers. Proceedings of the Symposium on Meteorological Observations from Space: Their Contribution to the First GARP Global Experiment, Committee on Space Research of the International Council of Scientific Unions, Philadelphia, 94-97.

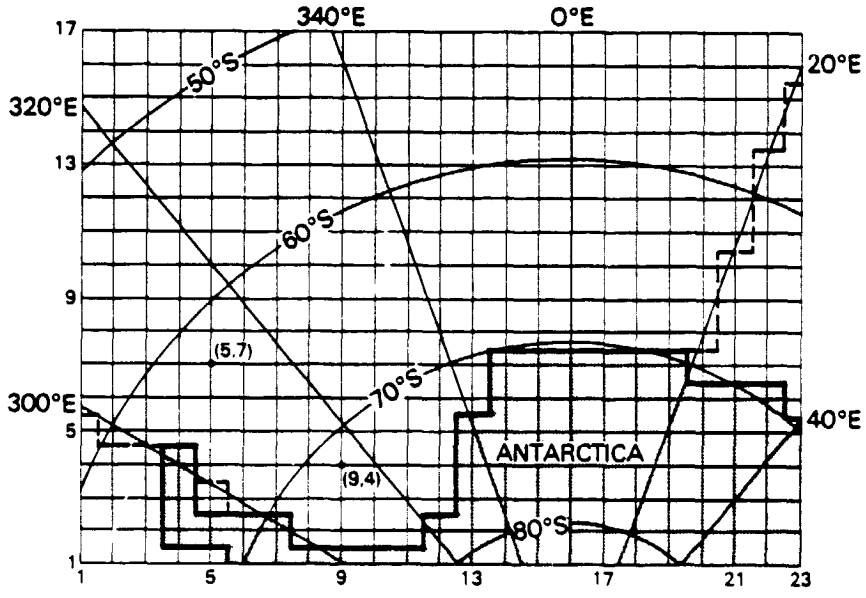

Figure 1. Grid structure of the model. The dashed lines at 20°E and 300°E define the boundaries of the Weddell Sea Sector.

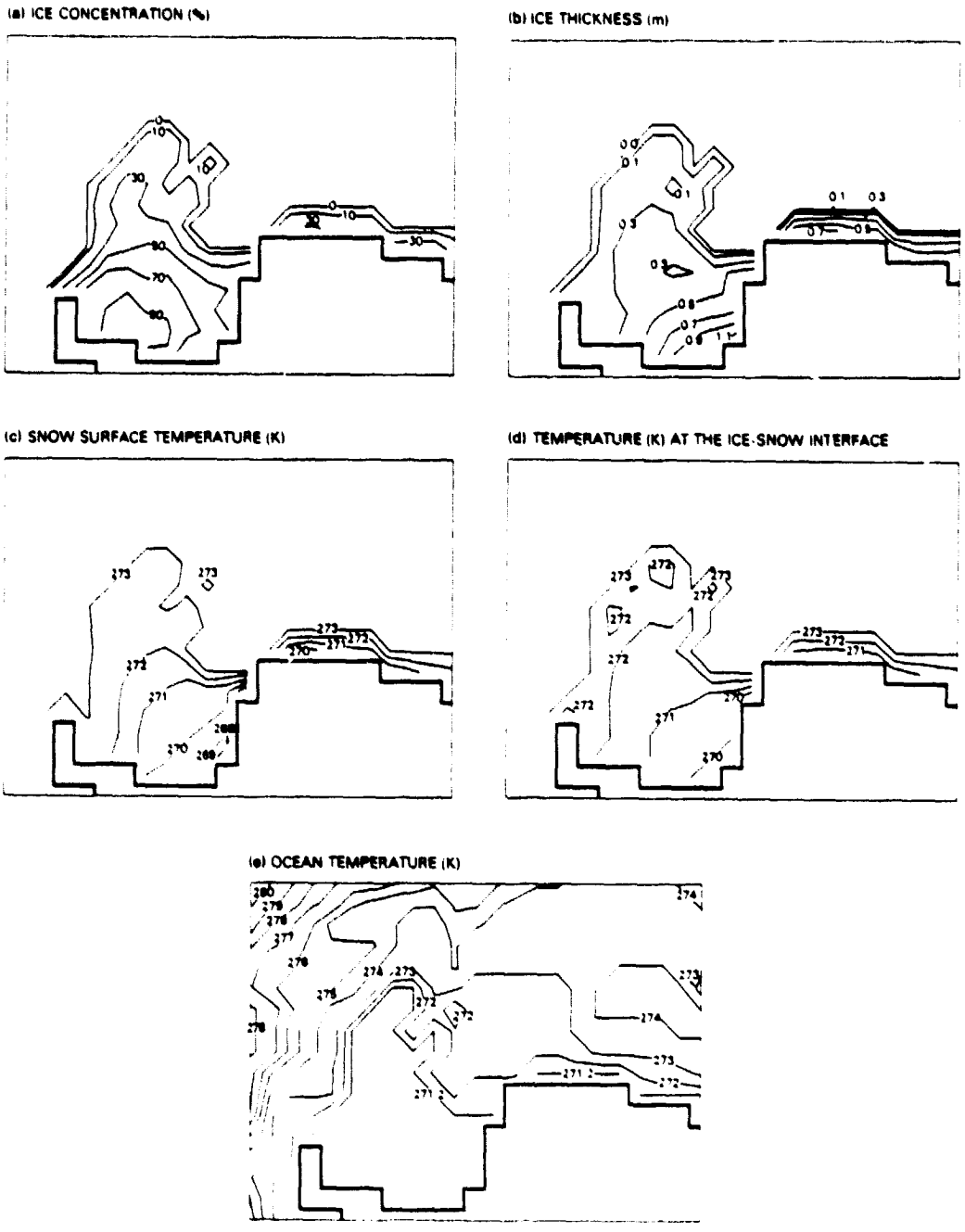

Figure 2. Contour maps of the initial conditions used for the model calculations:

(a) ice concentrations derived from ESMR satellite imagery;
(b) ice thicknesses calculated for January 1 from a 4-year simulation of the Parkinson and Washington (1979) model;
(c) snow-surface temperatures calculated for January 1 from a 4-year simulation of the Parkinson and Washington (1979) model;
(d) ice-snow interface temperatures calculated for January 1 from a 4-year simulation of the Parkinson and Washington (1979) model;
(e) ocean temperatures from the summertime 20 m values of Gordon and Goldberg (1970).

ICE THICKNESS (m) FOR FEBRUARY, YEAR 1

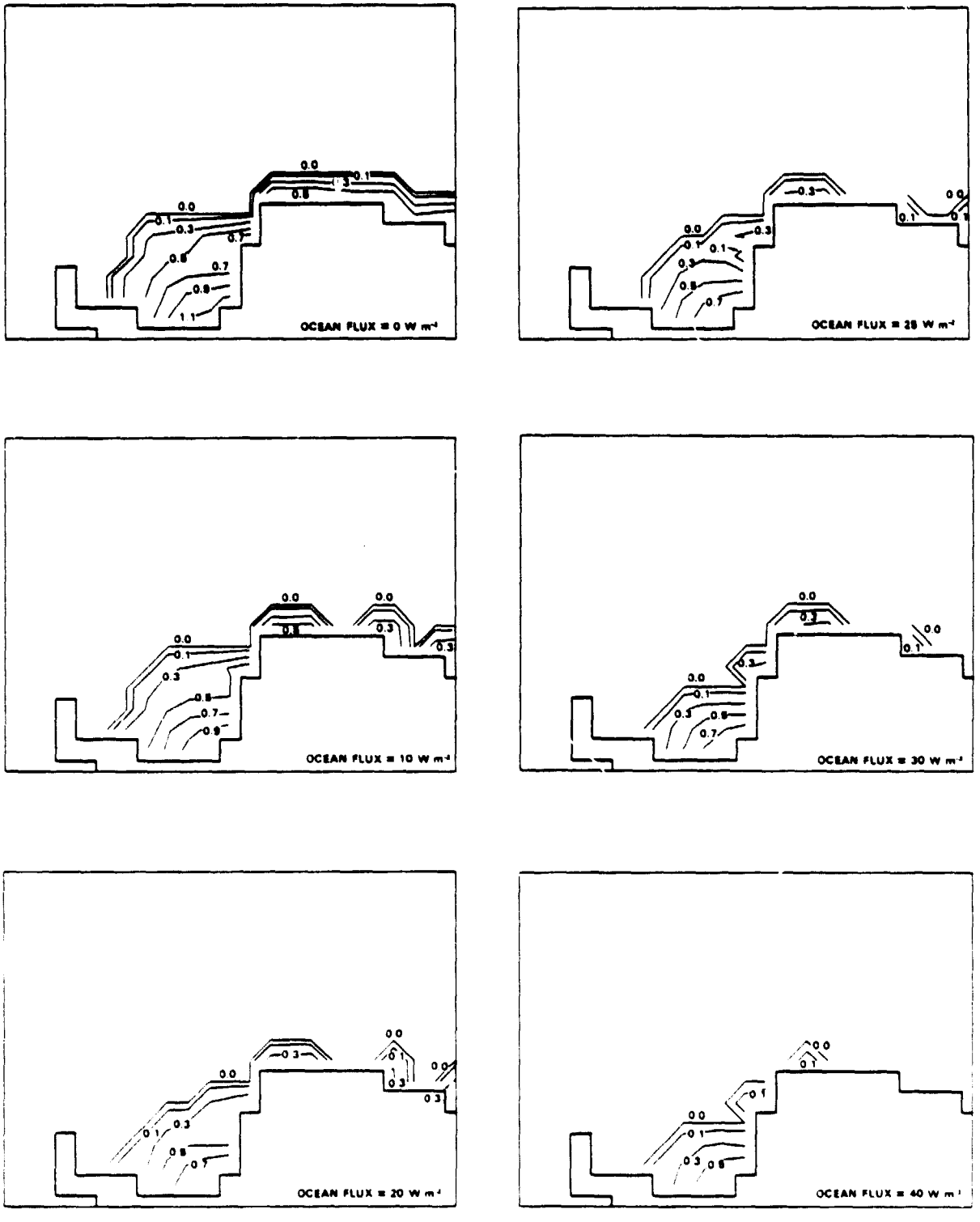

Figure 3. Contour maps of calculated ice thicknesses on February 15, year 1, for six values of the ocean heat flux.

ICE CONCENTRATION (%) FOR FEBRUARY, YEAR 1

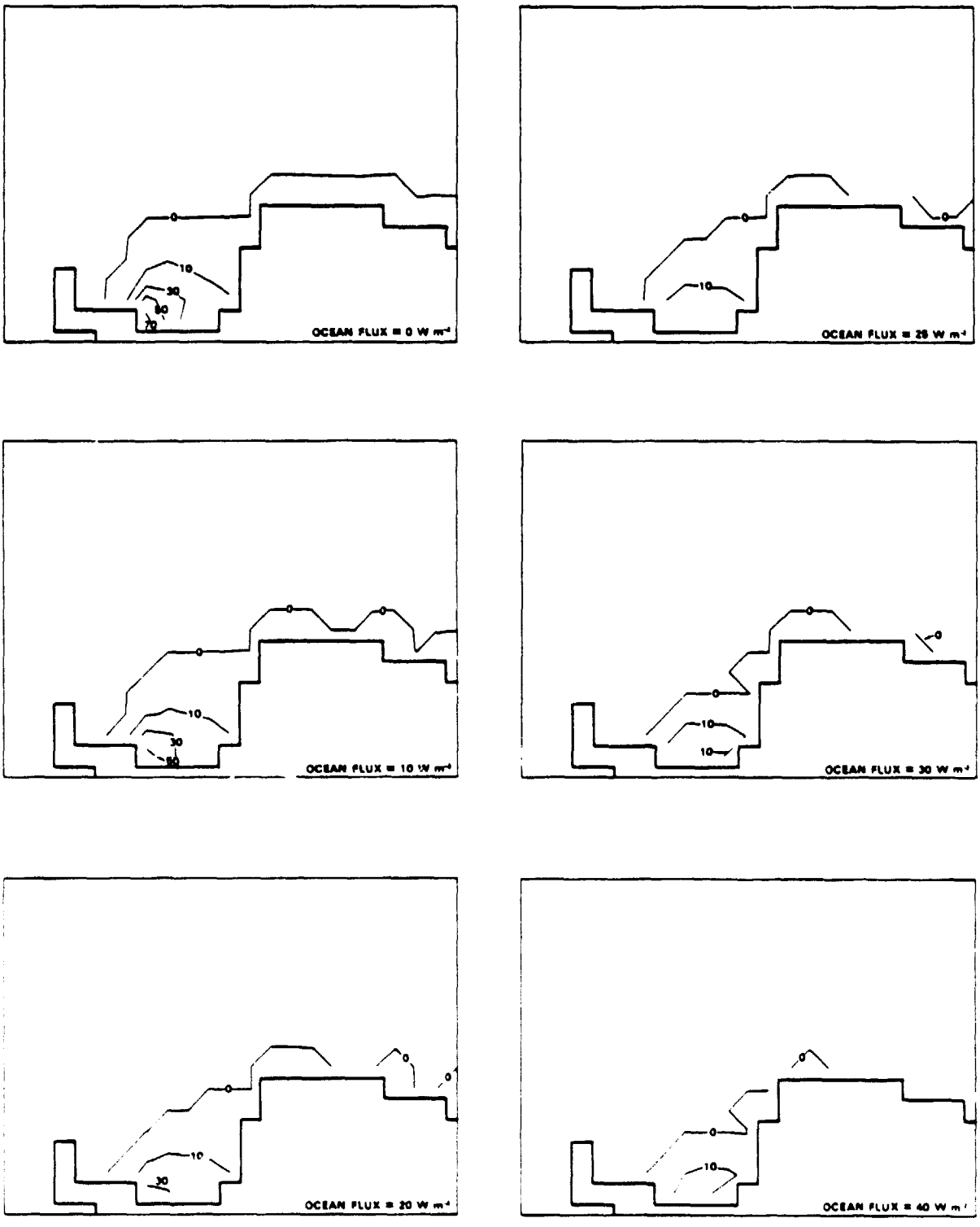

Figure 4. Contour maps of calculated ice concentrations on February 15, year 1, for six values of the ocean heat flux.

ICE THICKNESS (m) FOR AUGUST, YEAR 1

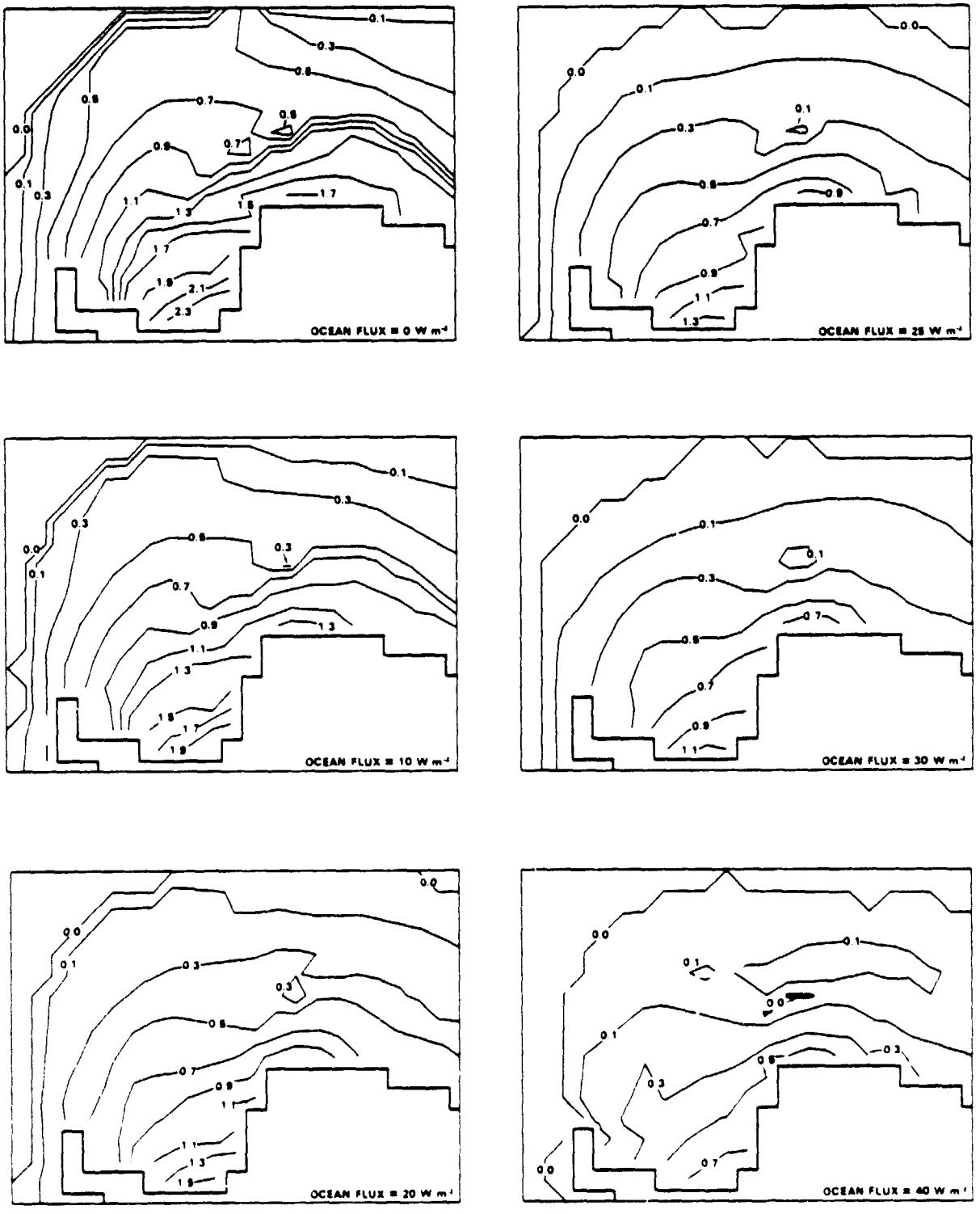

Figure 5. Contour maps of calculated ice thicknesses on August 15, year 1, for six values of the ocean heat flux.

ICE CONCENTRATION (%) FOR AUGUST, YEAR 1

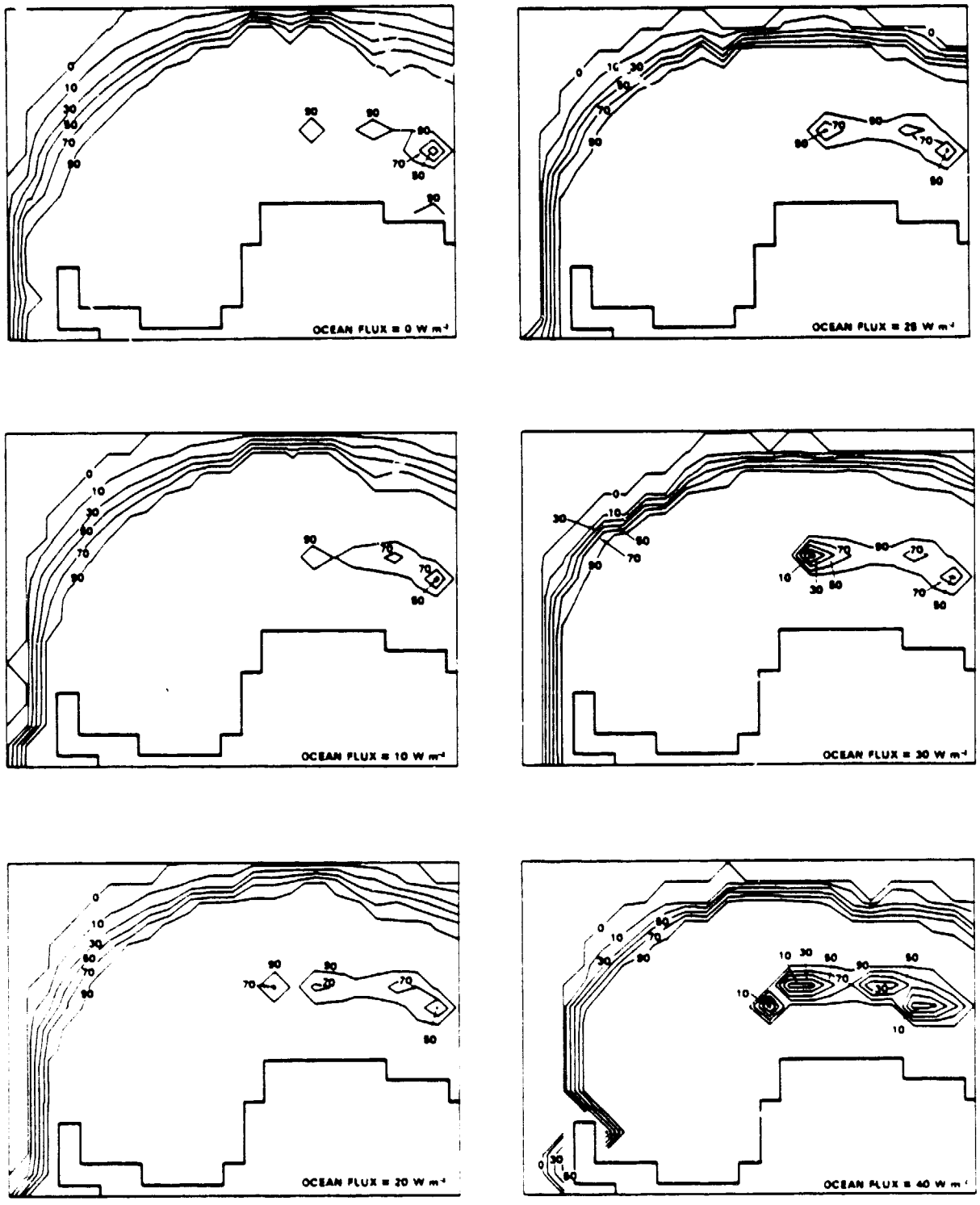

Figure 6. Contour maps of calculated ice concentrations on August 15, year 1, for six values of the ocean heat flux.

ICE THICKNESS (m) FOR FEBRUARY, YEAR 2

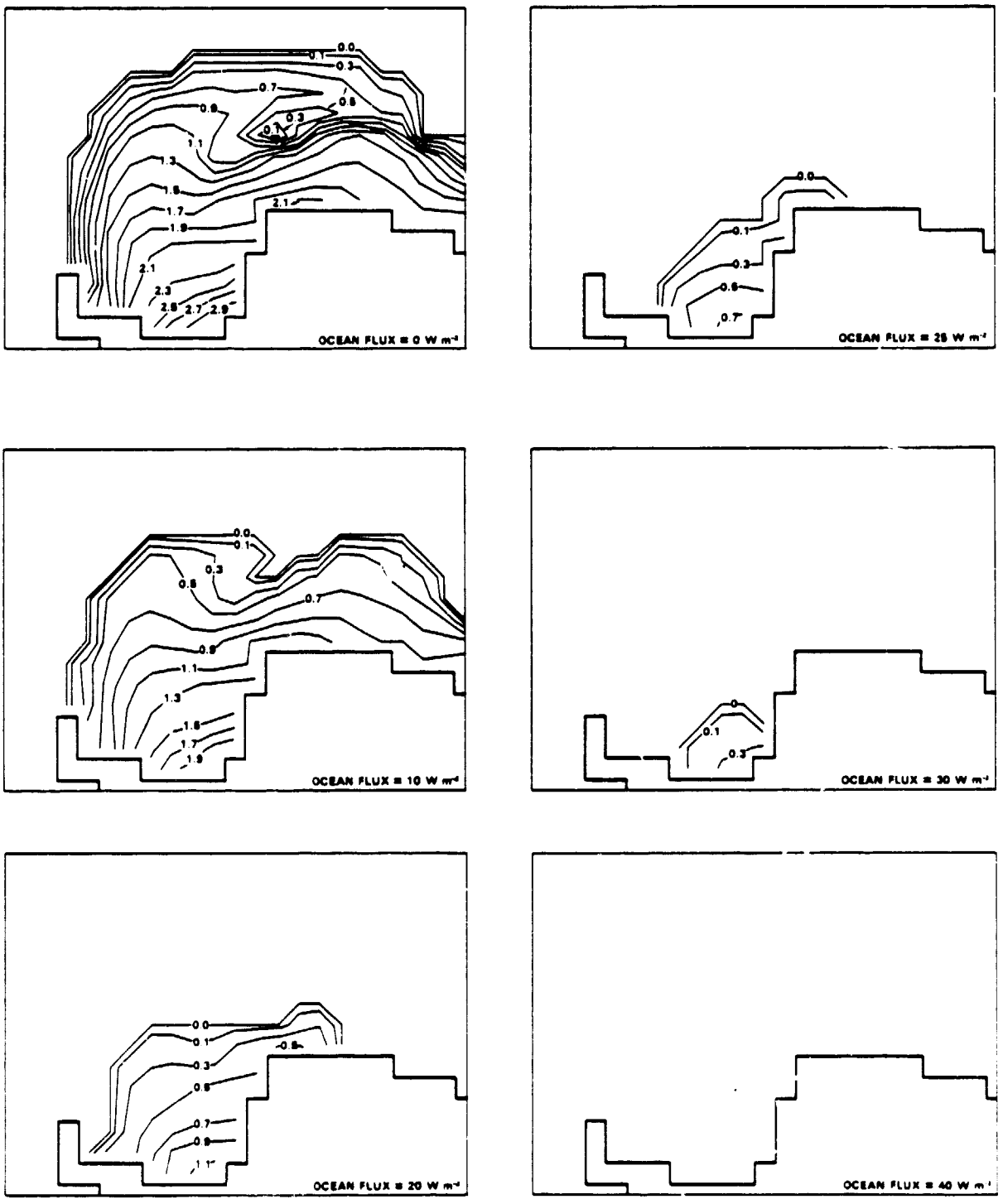

Figure 7. Contour maps of calculated ice thicknesses on February 15, year 2, for six values of the ocean heat flux.

ICE CONCENTRATION (%) FOR FEBRUARY, YEAR 2

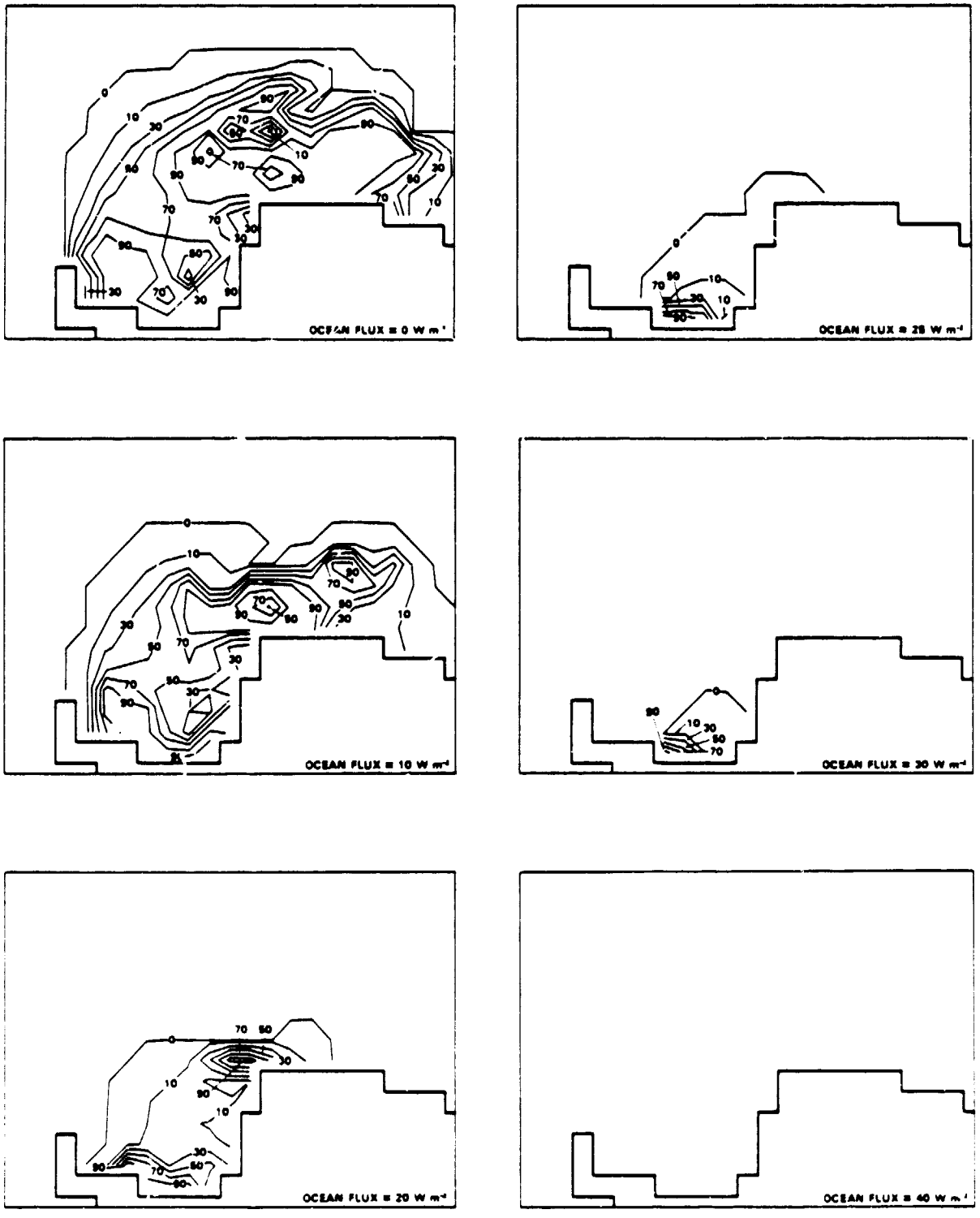

Figure 8. Contour maps of calculated ice concentrations on February 15, year 2, for six values of the ocean heat flux.

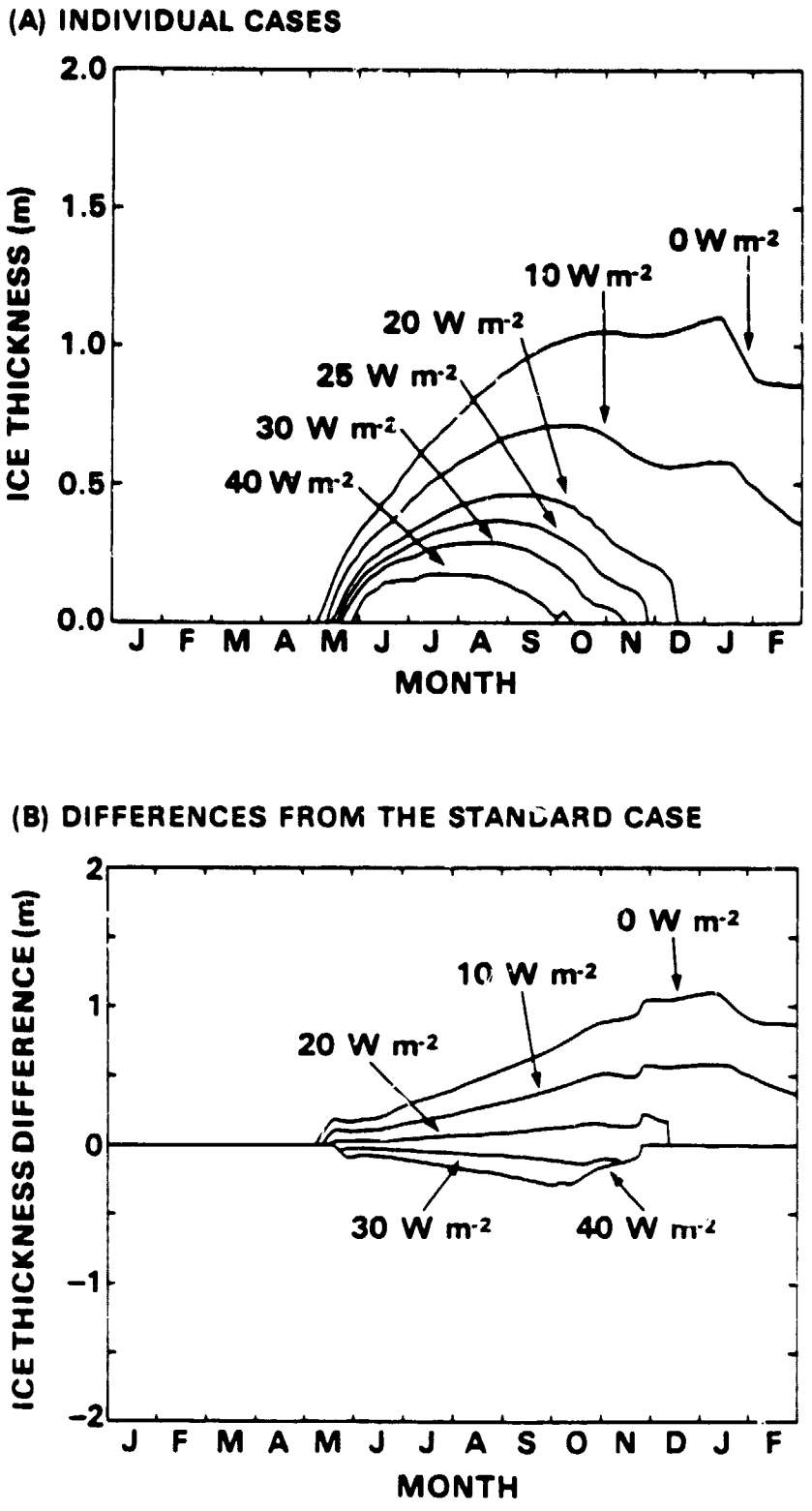

Figure 9. Time sequences of ice thickness at point (5,7):

(a) magnitudes for each of six values of the ocean heat flux;
(b) differences from the thickness calculated with an ocean flux of 25 W m^{-2}.

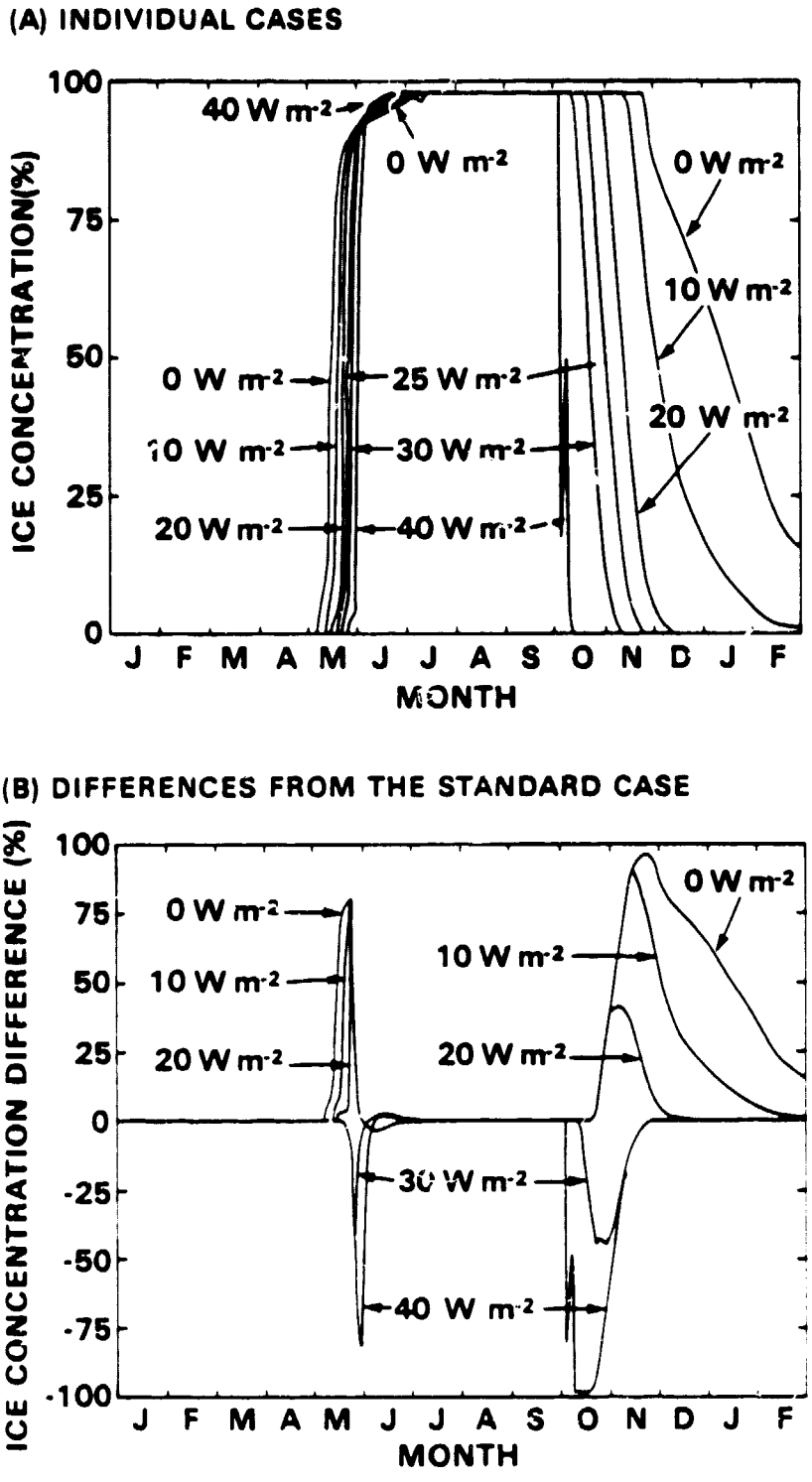

Figure 10. Time sequences of ice concentration at point (5,7):

(a) magnitudes for each of six values of the ocean heat flux;
(b) differences from the ice concentration calculated with an ocean flux of 25 W m^{-2}.

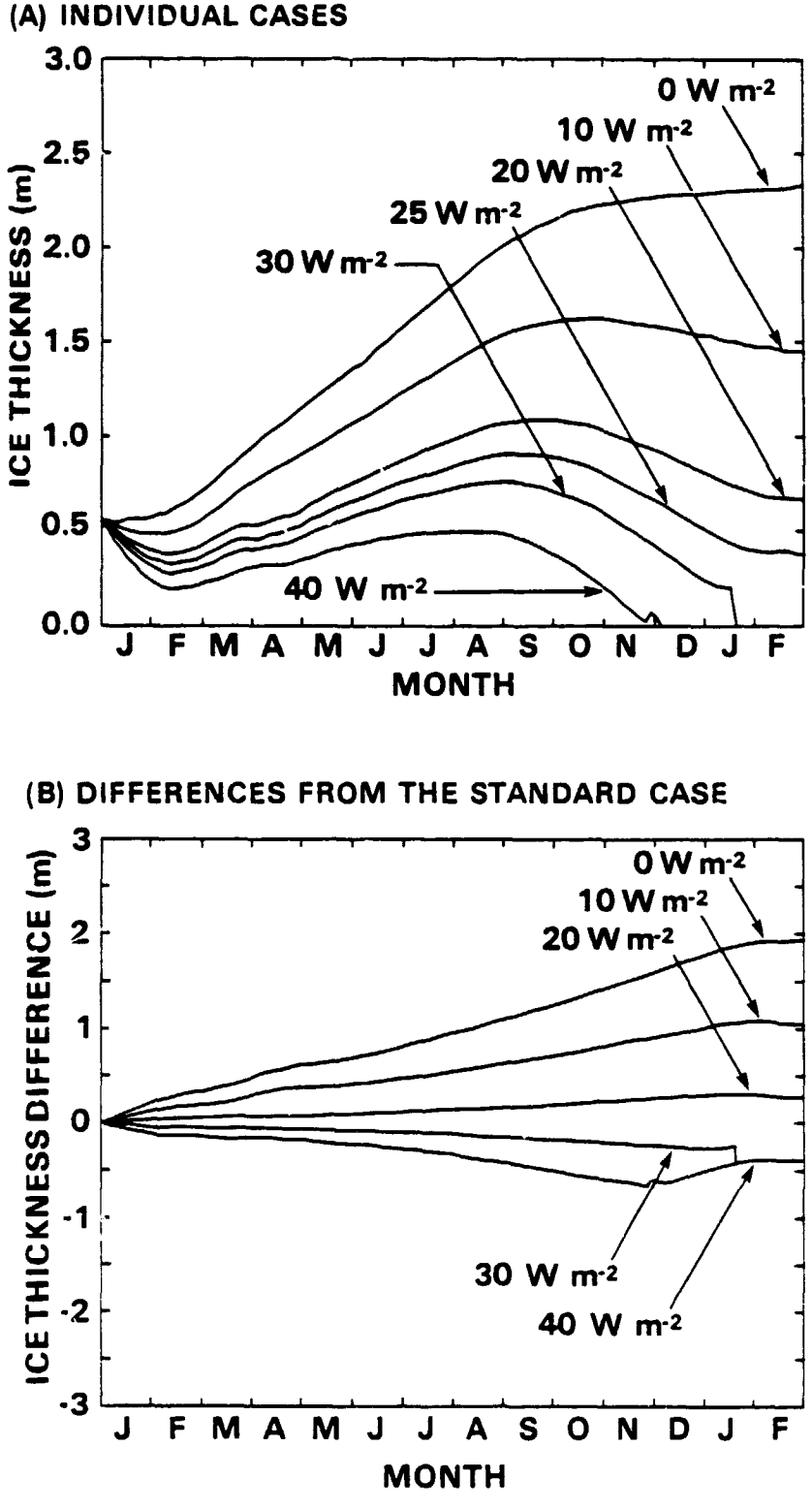

Figure 11. Time sequences of ice thickness at point (9,4):

(a) magnitudes for each of six values of the ocean heat flux;
(b) differences from the ice thickness calculated with an ocean flux of 25 W m^{-2}.

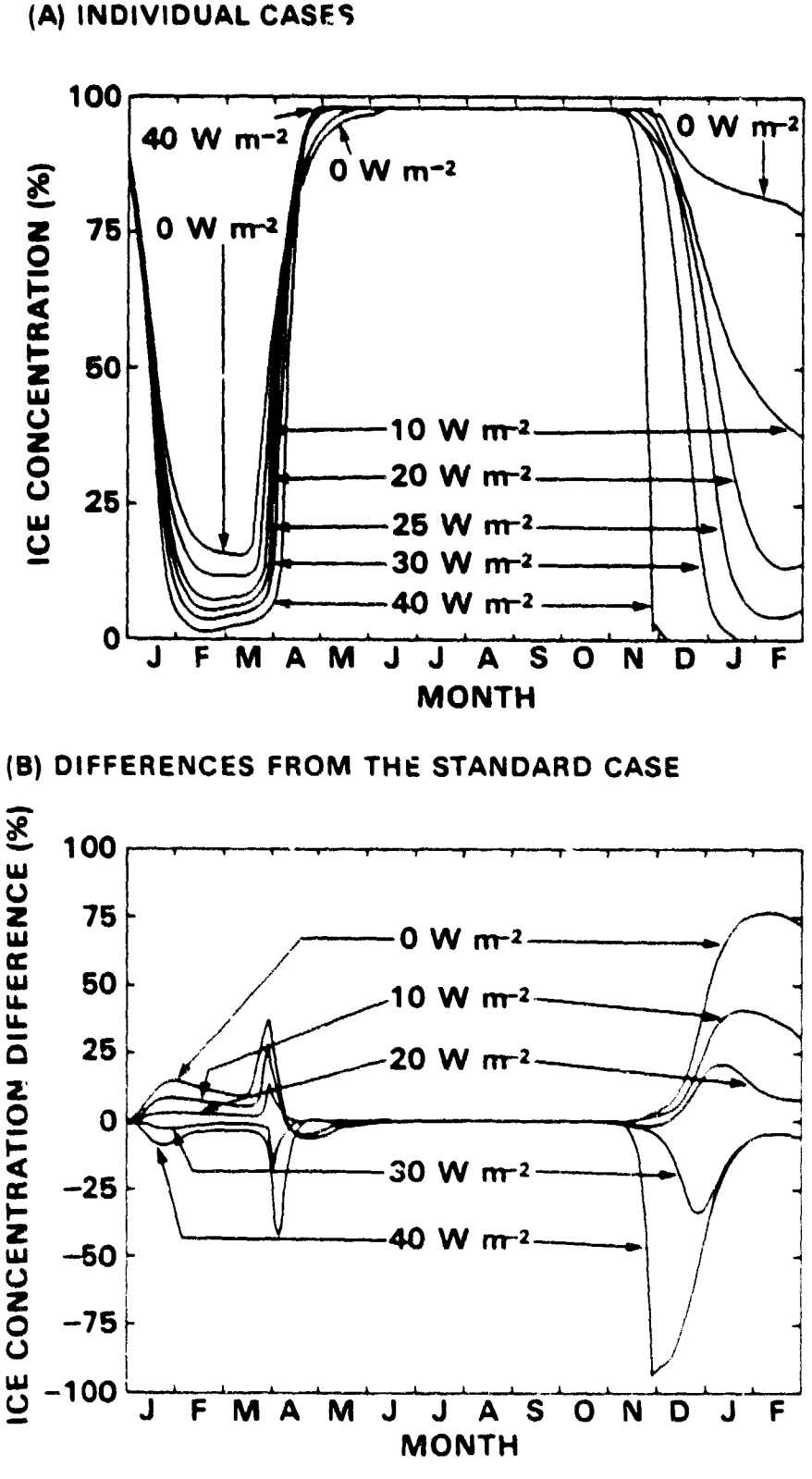

Figure 12. Time sequences of ice concentration at point (9,4):

(a) magnitudes for each of six values of the ocean heat flux;
(b) differences from the ice concentration calculated with an ocean flux of 25 W m^{-2}.

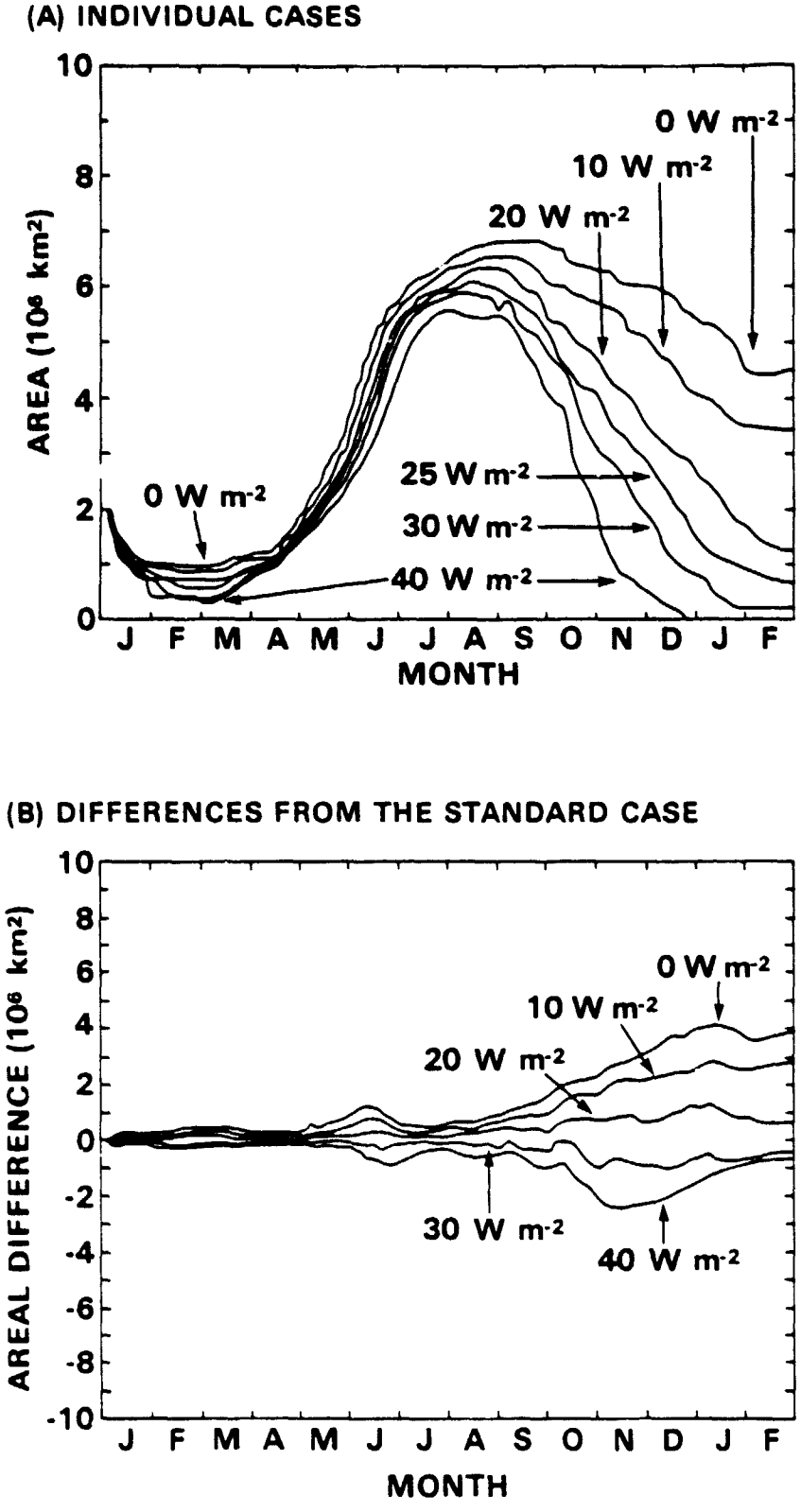

Figure 13. Time sequences of the area of ice-laden waters in the Weddell Sector:

(a) magnitudes for each of six values of the ocean heat flux;
(b) differences from the area of ice-laden waters calculated with an ocean flux of 25 W m-2.

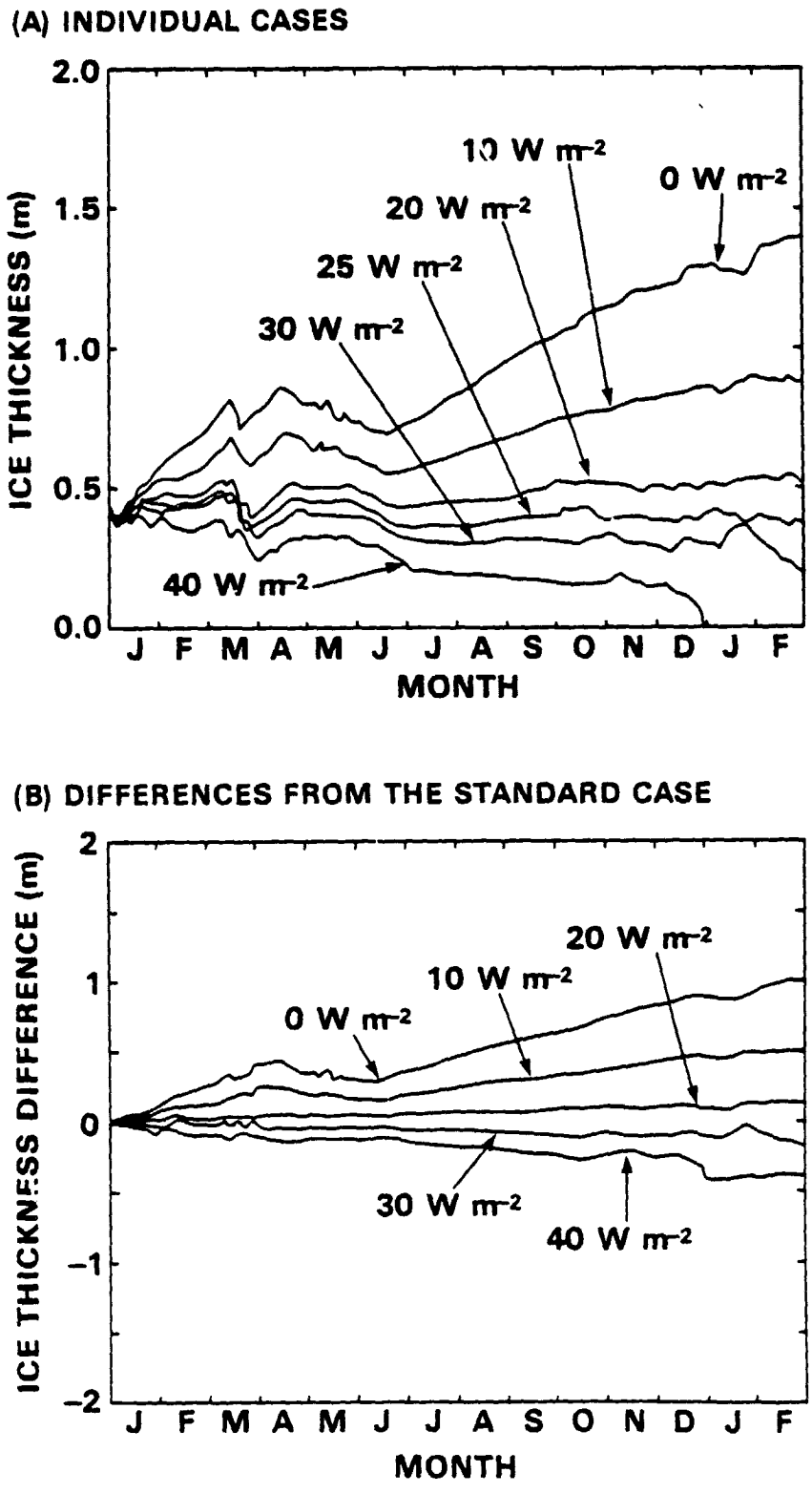

Figure 14. Time sequences of the mean ice thickness averaged over all ice-laden grid squares in the Weddell Sector:

(a) magnitudes for each of six values of the ocean heat flux;
(b) differences from the mean ice thickness calculated with an ocean flux of 25 W m^{-2}.

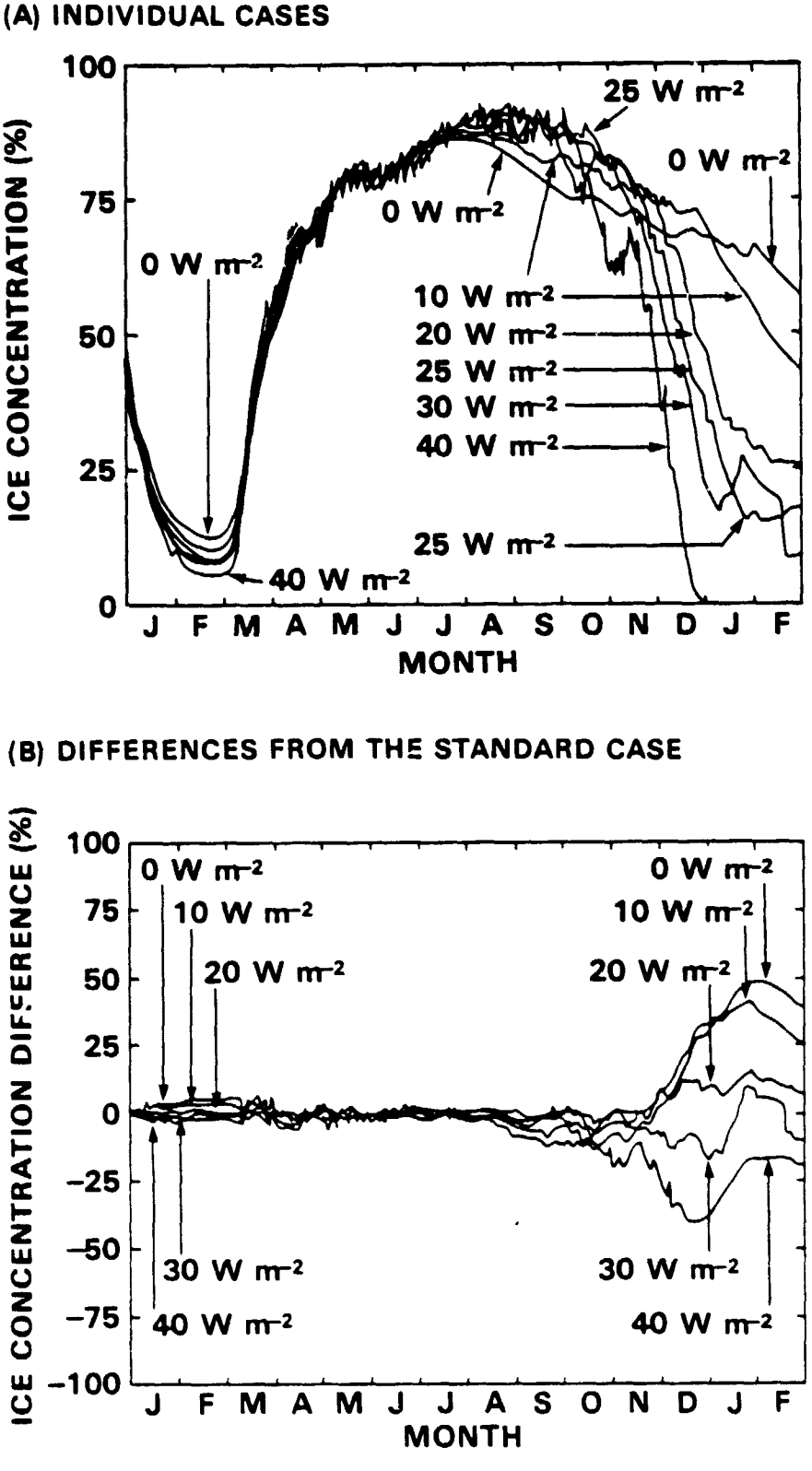

Figure 15. Time sequences of the mean ice concentrations averaged over all ice-laden grid squares in the Weddell Sector:

(a) magnitudes for each of six values of the ocean heat flux;
(b) differences from the mean ice concentration calculated with an ocean flux of 25 W m-2.

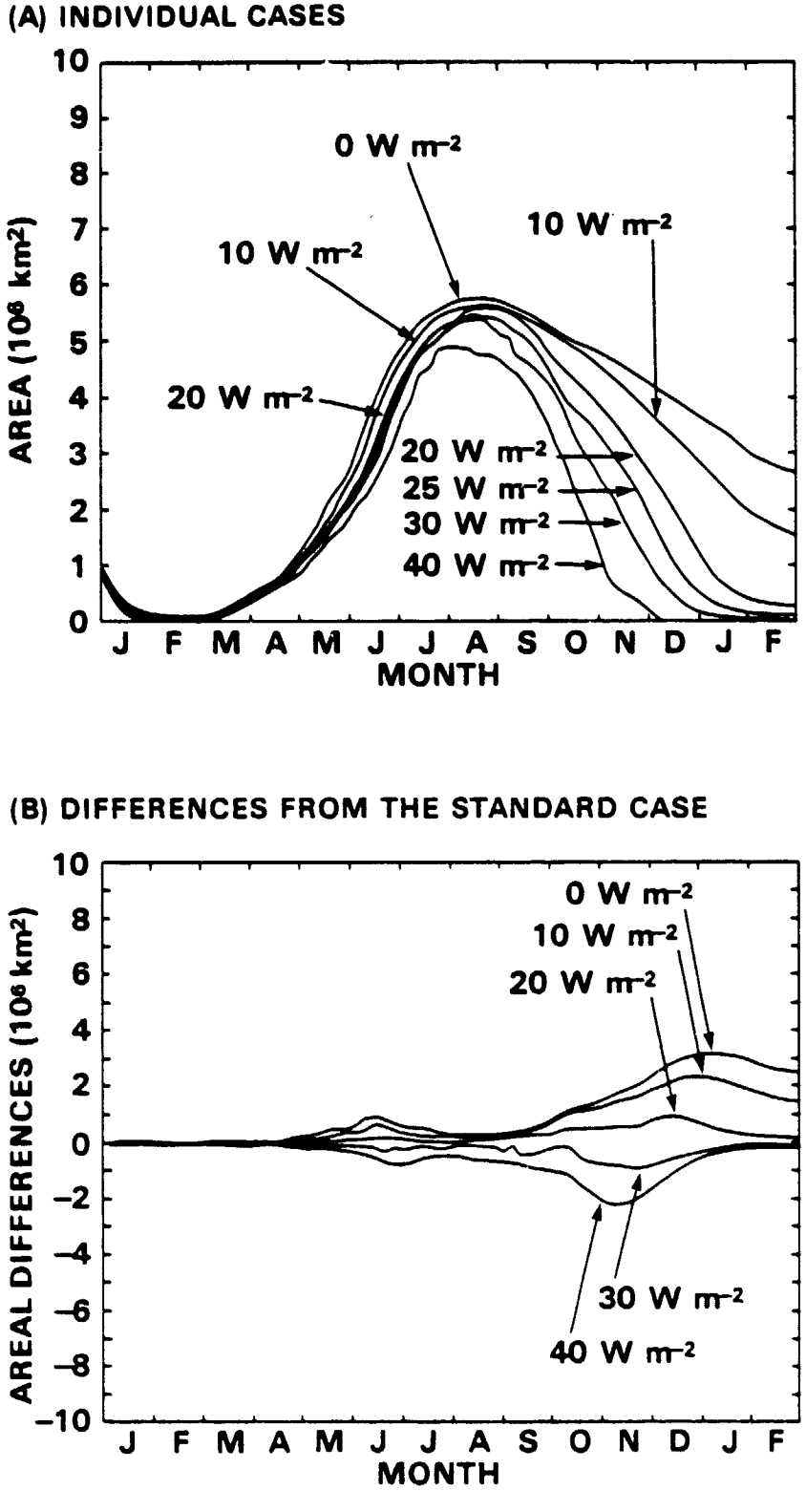

Figure 16. Time sequences of the cumulative ice area in the Weddell Sector:

(a) magnitudes for each of six values of the ocean heat flux;
(b) differences from the cumulative ice area calculated with an ocean flux of 25 W m^{-2}.